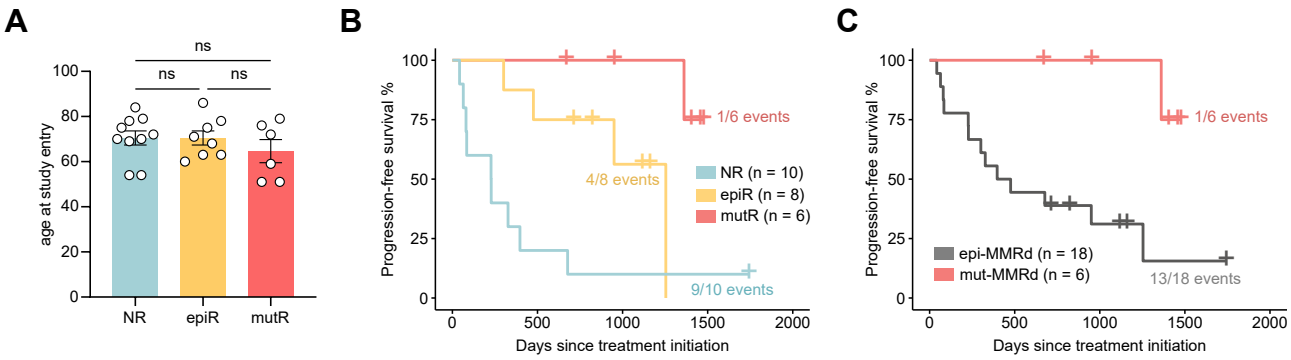

Supplementary Figure S1: Additional characterization of the clinical trial cohort

A. Bar plot detailing the age of trial participants at the time of study entry, across NR, epiR, and mutR groups. Statistical significance was assessed by one-way ANOVA with Tukey's multiple comparisons test.

B-C. Kaplan-Meier progression-free survival curves, separated by NR, epiR, and mutR classifications (**B**), or by the mechanism of MMRd (**C**), calculated relative to the timepoint of pembrolizumab initiation in each patient. The proportion of patients that showed progression of disease is also annotated.

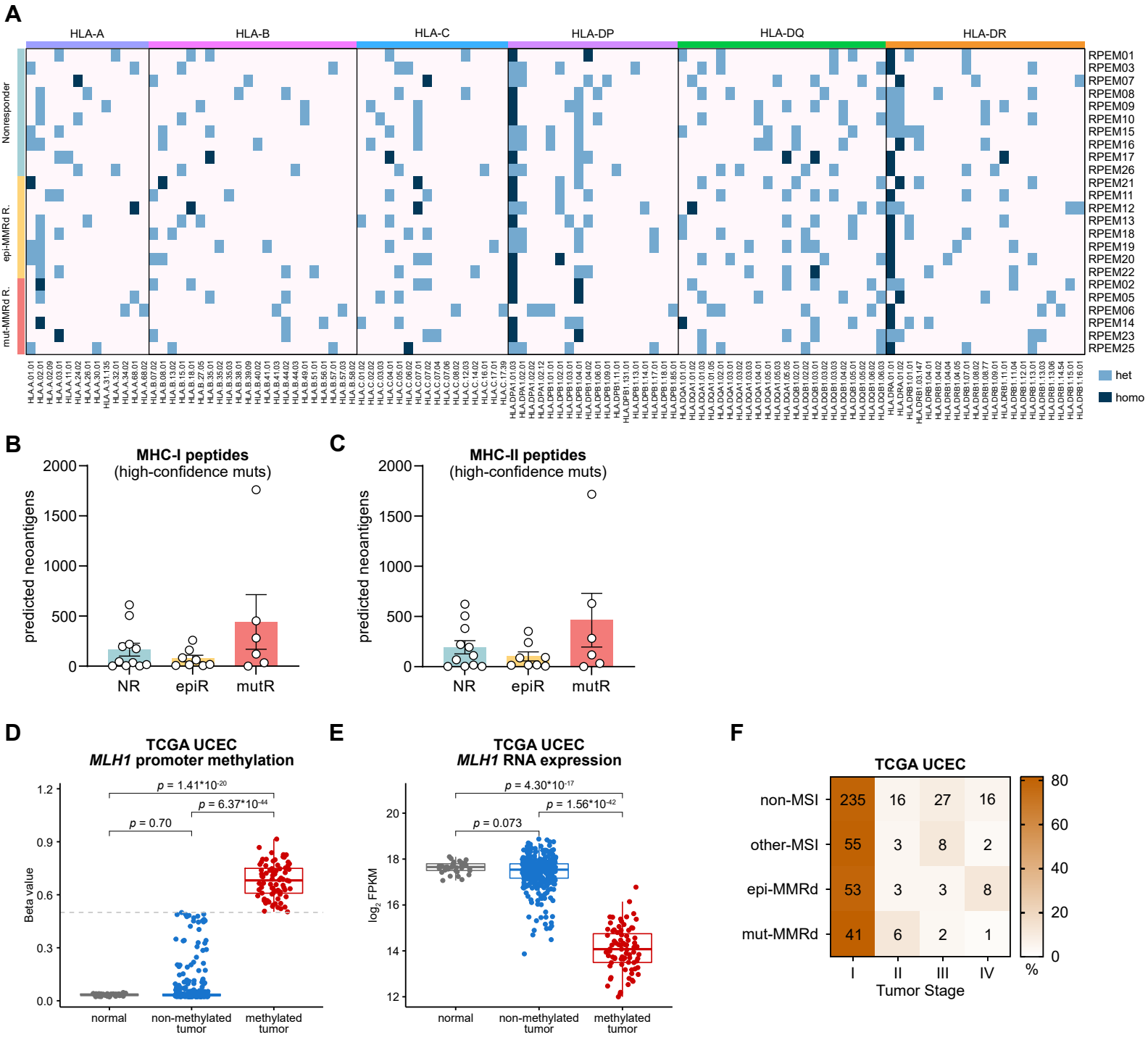

Supplementary Figure S2: Additional characterization of exome profiles and defining *MLH1* methylation status

A. HLA genotypes in each sample, defined for HLA-A, HLA-B, HLA-C, HLA-DP, HLA-DQ, and HLA-DR. Light blue cells indicate heterozygosity, while dark blue cells denote homozygosity.

B-C. Number of predicted neoantigens for MHC-I (**B**) or MHC-II (**C**) in each pre-treatment sample, based on the exome profiles.

D. Tukey boxplots of composite methylation beta values for probes tiling the *MLH1* promoter. Data are from the TCGA UCEC cohort. A beta value threshold of 0.5 was used to define non-methylated and methylated tumors. Statistical significance was assessed by two-tailed unpaired Mann-Whitney test.

E. Expression of *MLH1* in the TCGA UCEC cohort, stratified by *MLH1* promoter methylation status, as in (**D**). Statistical significance was assessed by two-tailed unpaired Mann-Whitney test.

F. Heatmap of tumor stage annotations across groups. Cells are colored by the percentage of patients within each patient category, with the number of patients indicated in each cell.

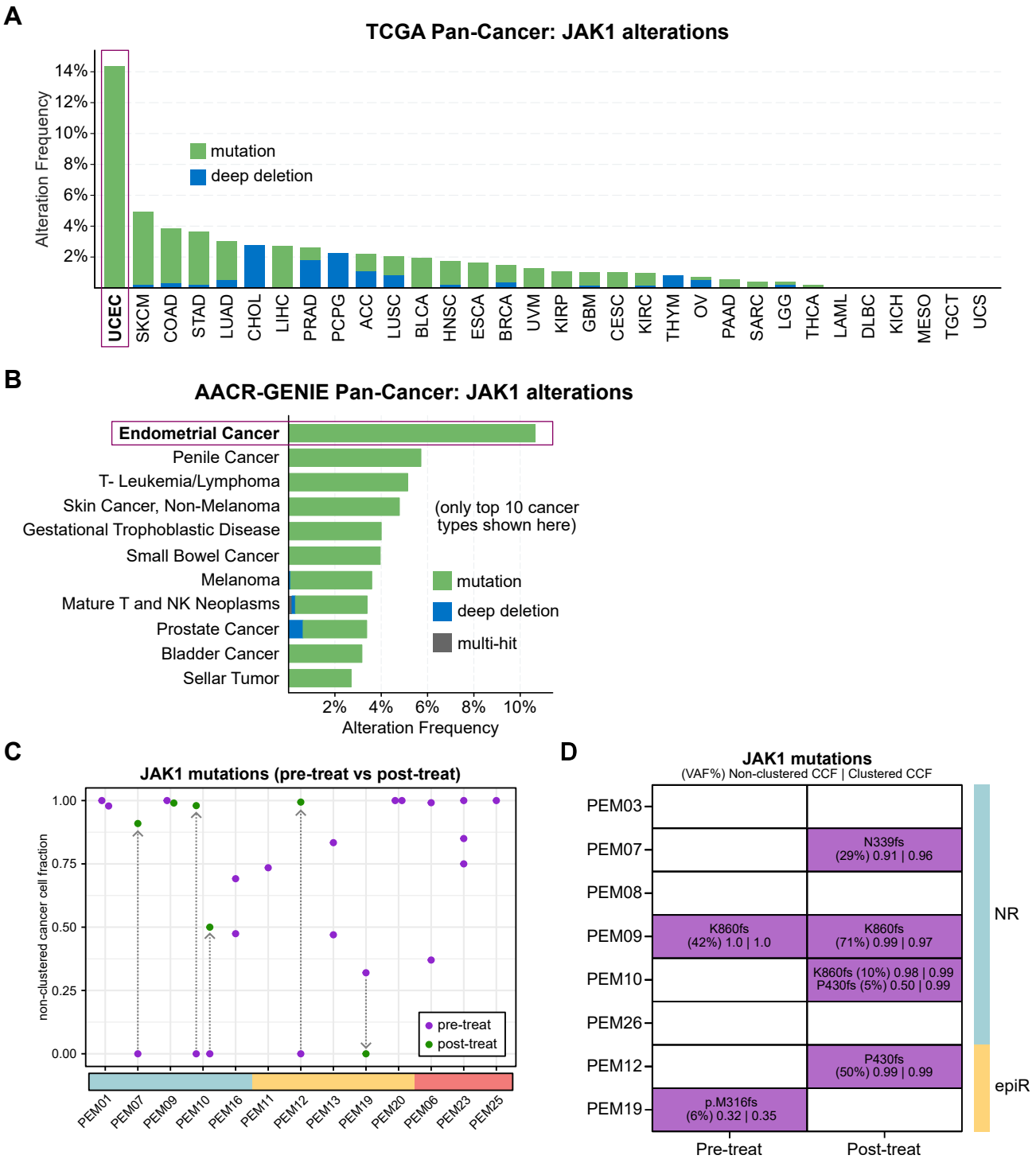

Supplementary Figure S3: *JAK1* alterations are most frequent in endometrial cancer

A. Alteration frequency of *JAK1* across the TCGA Pan-Cancer Atlas.

B. Alteration frequency of *JAK1* across the AACR-GENIE cohort.

C. *JAK1*-mutant cancer cell fractions (CCFs) in *JAK1*-mutant tumors, without clustering. Each point represents a unique *JAK1* variant that was identified in a particular sample. Pre-treatment CCFs are annotated in purple, while post-treatment CCFs are in green, with arrows that connect the same variant across timepoints.

D. *JAK1* mutations in 8 patients from the trial cohort with matched pre-treatment and post-treatment tumor exomes. Samples with a *JAK1* mutation are shaded purple, with the specific mutation annotated. Variant allele frequencies (VAFs) are shown, along with estimated cancer cell fractions (CCFs; non-clustered and clustered).

A

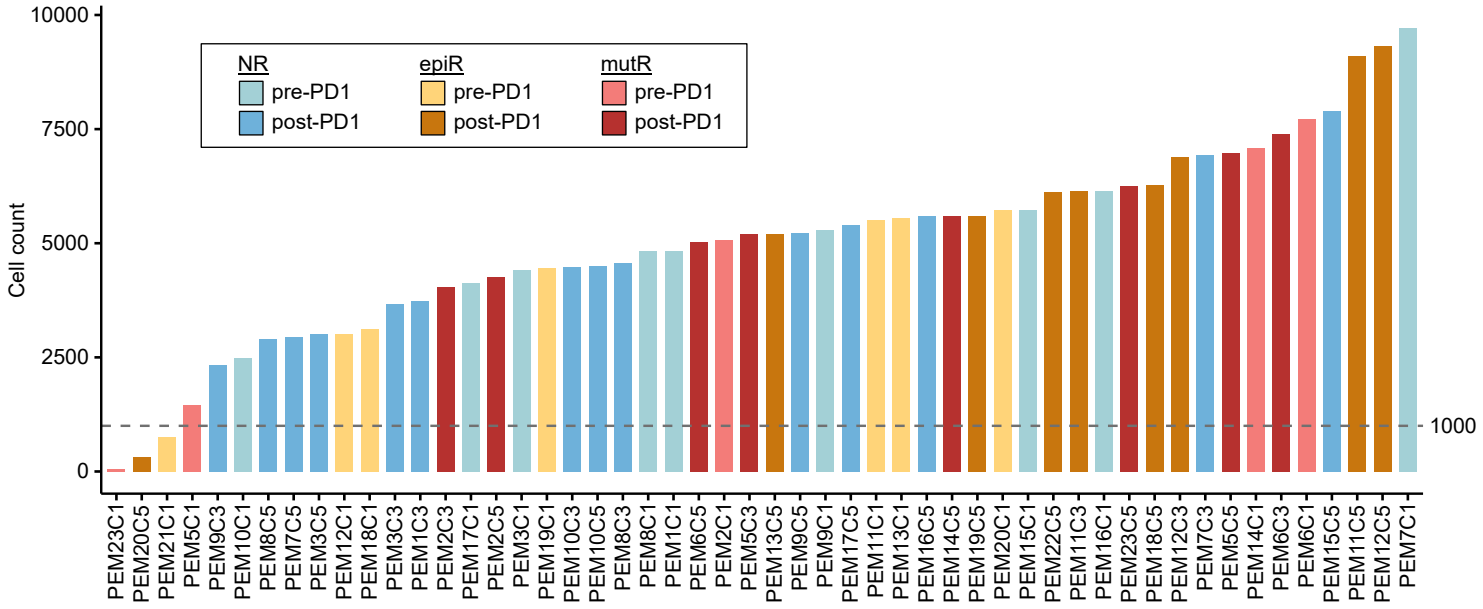

Supplementary Figure S4: Final cell counts in each scRNA-seq sample

A. Bar plot showing the number of cells passing filtering criteria for each sample in the scRNA-seq dataset. After quality control and cell filtering, samples with fewer than 1000 cells were removed from further analysis.

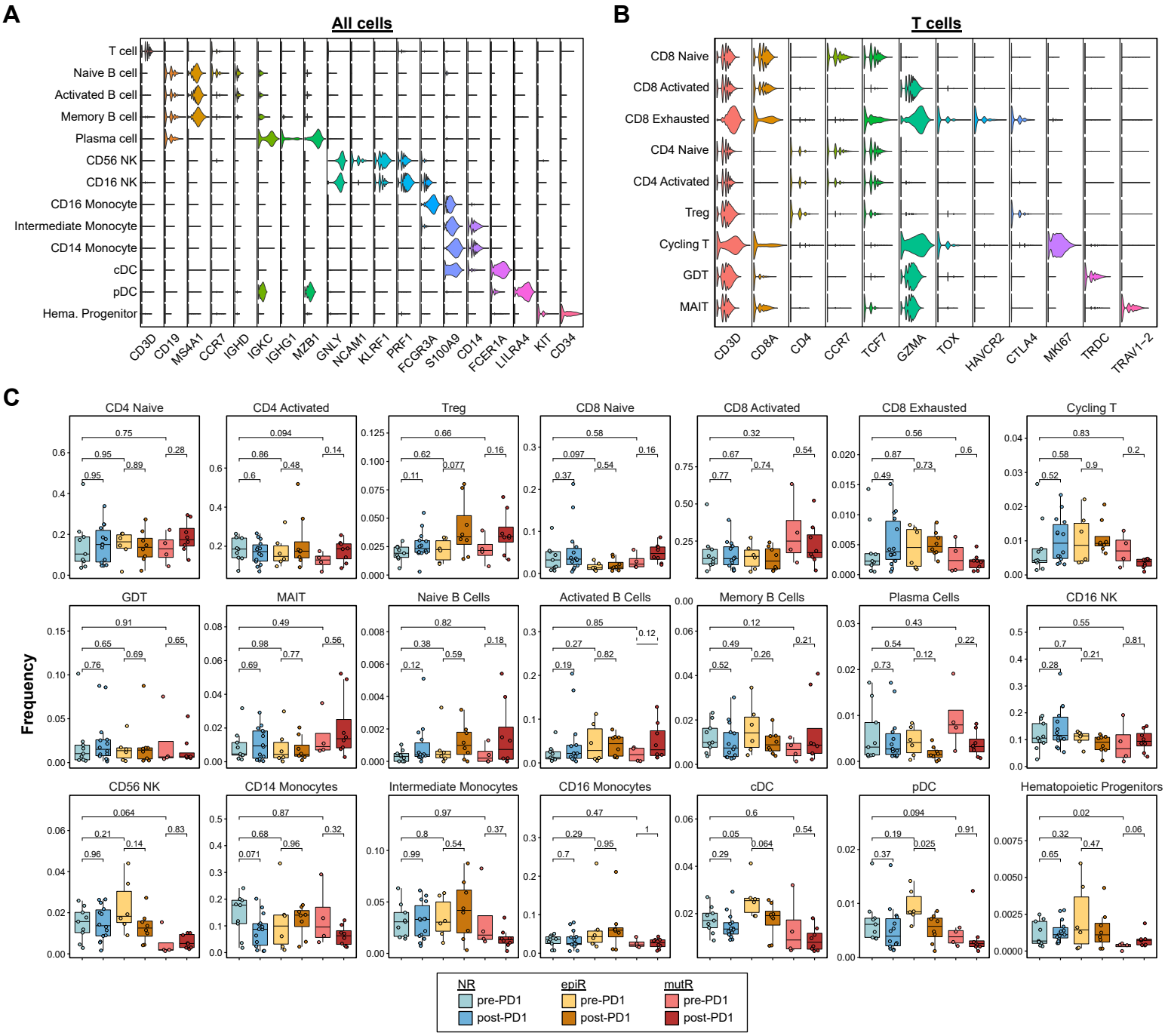

Supplementary Figure S5: Longitudinal transcriptional profiling of circulating immune cells before and after PD-1 blockade

A. Violin plots detailing key marker genes for each of the cell types identified in **Figure 3A**.

B. Violin plots detailing key marker genes for each of the T cell subsets identified in **Figure 3B**.

C. Tukey boxplots of total frequencies for each of the 21 cell types. Each point represents one sample, either before or after PD-1 immunotherapy. Statistical significance was assessed by two-tailed unpaired t-test.

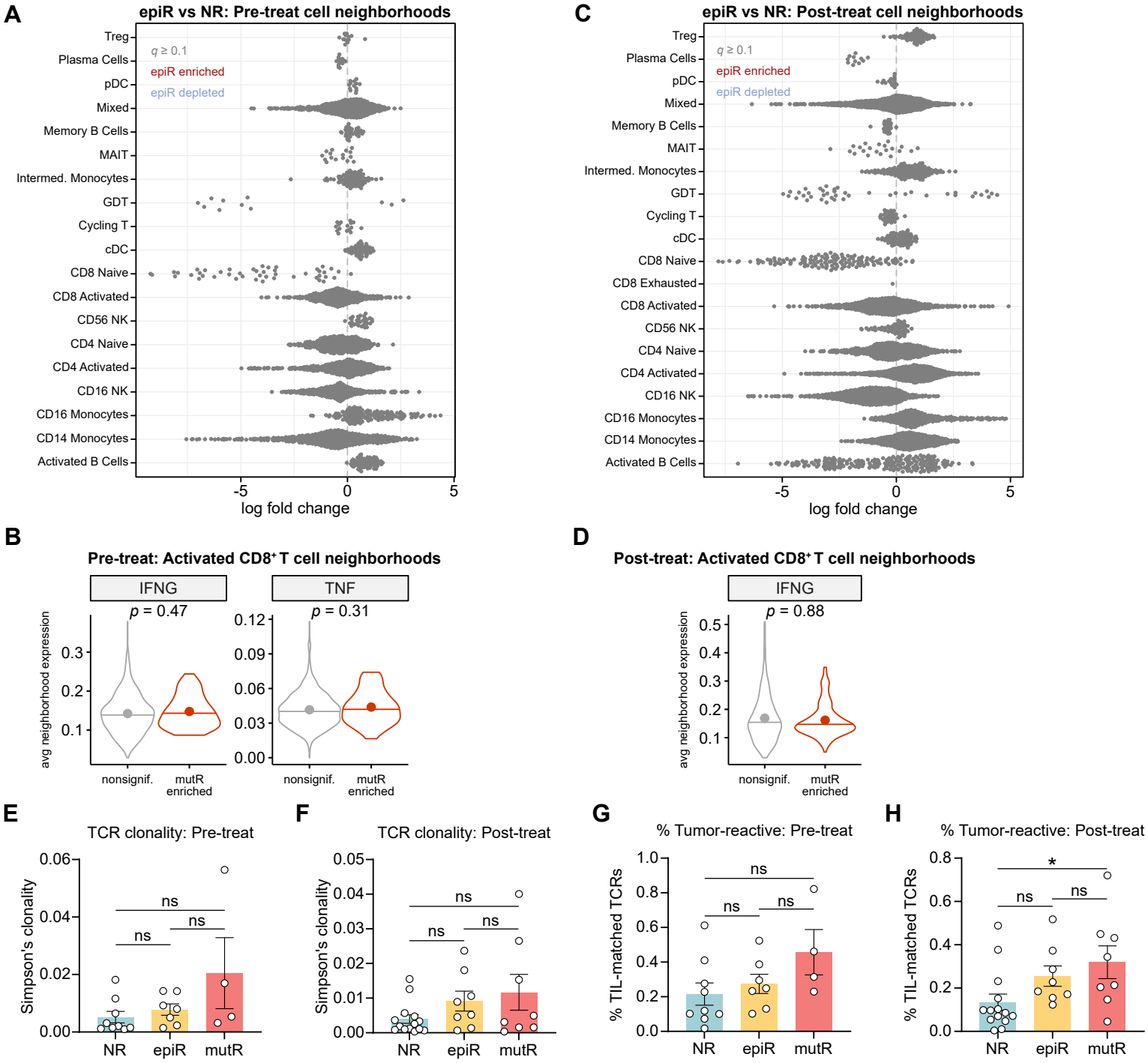

Supplementary Figure S6: Differential abundance of cell neighborhoods after PD-1 immunotherapy

A. Milo differential abundance analysis for in epiR vs NR patients, before PD-1 immunotherapy.

B. Violin plots of *IFNG* and *TNF* expression in activated CD8⁺ T cell neighborhoods that are enriched in mutR vs NR patients, before PD-1 immunotherapy. Horizontal lines indicate the median, while points indicate the mean.

C. Milo differential abundance analysis in epiR vs NR patients, after PD-1 immunotherapy.

D. Violin plots of *IFNG* expression in activated CD8⁺ T cell neighborhoods that are enriched in mutR vs NR patients, after PD-1 immunotherapy. Horizontal lines indicate the median, while points indicate the mean.

E-F. Simpson's clonality indices of peripheral TCR repertoires before (**E**) or after (**F**) PD-1 immunotherapy.

G-H. The percentage of peripheral TCR sequences matched to pre-treatment tumor-infiltrating TCR repertoires, before (**G**) or after (**H**) PD-1 immunotherapy.

In (**A**) and (**C**), statistical significance was determined through a generalized linear model with Benjamini-Hochberg multiple hypothesis correction, as implemented in Milo. In (**B**) and (**D**), statistical significance was assessed by two-sided Mann-Whitney test, with Benjamini-Hochberg multiple hypothesis correction. In **E-H**, statistical significance was assessed by one-way ANOVA with Tukey's multiple comparisons test.

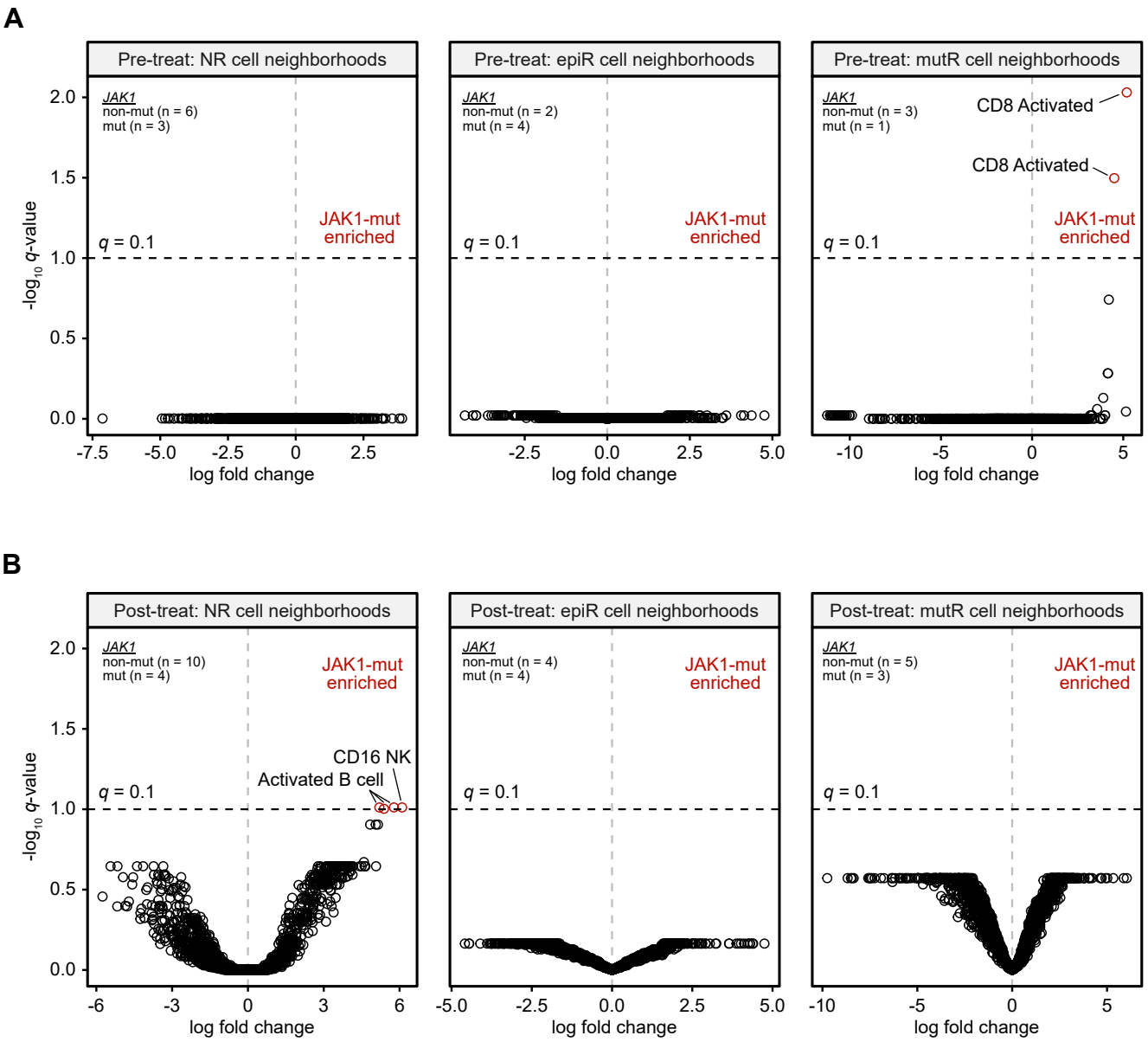

Supplementary Figure S7: Differential abundance of cell neighborhoods in *JAK1*-mutant tumors

A-B. Differential abundance analysis of cell neighborhoods in *JAK1*-mutant vs non-mutant tumors, before **(A)** or after (**B**) PD-1 immunotherapy. Cell neighborhoods were identified by kNN clustering, with each point representing one neighborhood. Neighborhoods in black were not significantly different compared to NR patients ($q \geq 0.1$); neighborhoods in red were enriched in *JAK1*-mutant samples. Statistical significance was determined through a generalized linear model, as implemented in Milo.

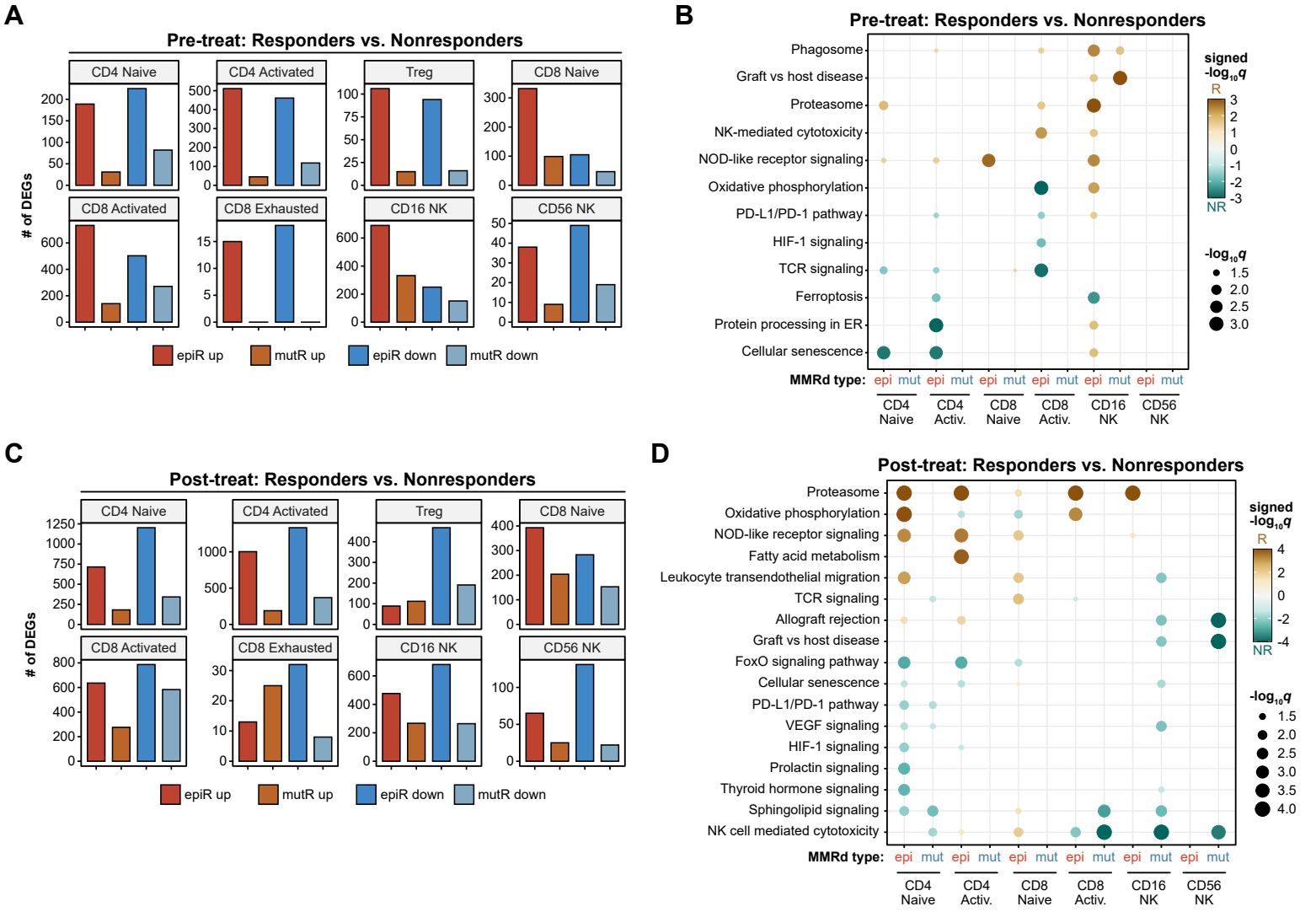

Supplementary Figure S8: Transcriptional profiles of T and NK cells in responders vs non-responders

A. The number of DEGs in T and NK cell populations from epiR or mutR patients compared to NR patients, before PD-1 immunotherapy.

B. Dot plots detailing significantly upregulated or downregulated pathways in each of the cell types, comparing epiR or mutR patients to NR patients, before PD-1 immunotherapy. Statistical significance was assessed by hypergeometric test with Benjamini-Hochberg multiple hypothesis correction, visualized as signed -$\log_{10}$ *q*-values.

C. The number of DEGs in T and NK cell populations from epiR or mutR patients compared to NR patients, after PD-1 immunotherapy.

D. Dot plots detailing significantly upregulated or downregulated pathways in each of the cell types, comparing epiR or mutR patients to NR patients, after PD-1 immunotherapy. Statistical significance was assessed by hypergeometric test with Benjamini-Hochberg multiple hypothesis correction, visualized as signed -$\log_{10}$ *q*-values.

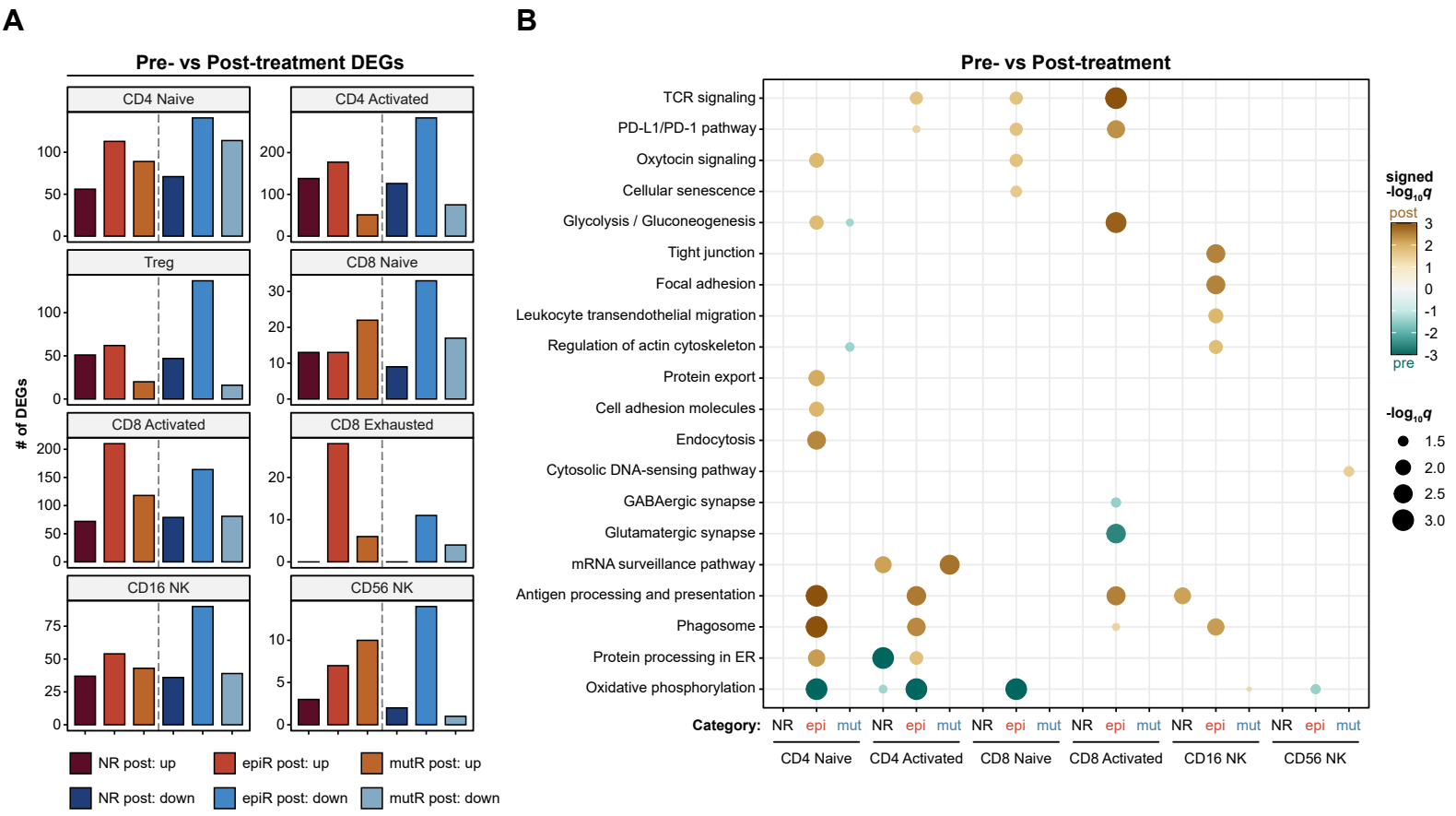

Supplementary Figure S9: Gene expression changes in T and NK cells following PD-1 immunotherapy

A. The number of DEGs in T and NK cell populations from NR, epiR, or mutR patients, comparing cells before and after PD-1 immunotherapy within each patient group.

B. Dot plot detailing significantly upregulated or downregulated pathways in each of the cell types, comparing cells from before and after PD-1 immunotherapy within each patient group. Statistical significance was assessed by hypergeometric test with Benjamini-Hochberg multiple hypothesis correction, visualized as signed -$\log_{10}$ *q*-values.

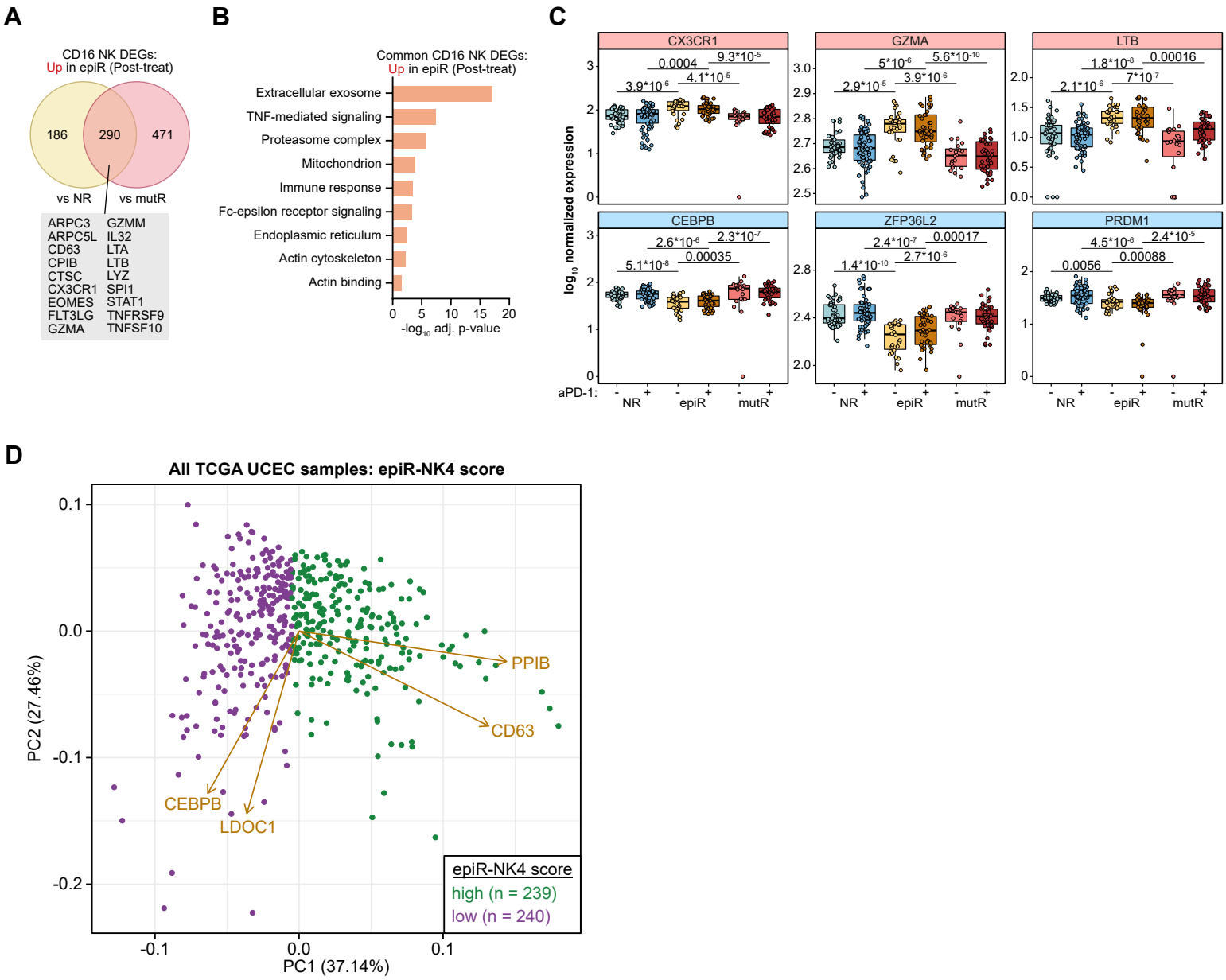

Supplementary Figure S10: Additional transcriptional characterization of CD16⁺ NK cells in epiR patients

A. Venn diagram of DEGs in CD16⁺ NK cells that are significantly upregulated in epiR patients compared to NR or mutR patients, after PD-1 immunotherapy.

B. Ontology enrichment analysis of DEGs in CD16⁺ NK cells that are significantly upregulated in epiR patients compared to NR or mutR patients, after PD-1 immunotherapy. Statistical significance was assessed by hypergeometric test with Benjamini-Hochberg multiple hypothesis correction.

C. Tukey boxplots of normalized gene expression values for select DEGs in epiR CD16⁺ NK cells.

D. Biplot of the principal component analysis used to construct the epiR-NK4 score from the TCGA UCEC cohort.